Materials Chemistry and Physics xxx (xxxx) 124546

Contents lists available at ScienceDirect

Materials Chemistry and Physics

journal homepage: www.elsevier.com/locate/matchemphys

A study of uncoated and coated nickel-zinc ferrite nanoparticles for magnetic hyperthermia

P.V. Ramana [a, b, *], K. Srinivasa Rao [c], K. Raghu Kumar [d], Govinda Kapusetti [e, **], Mounika Choppadandi [e], J.N. Kiran [f], K.H. Rao [b]

[a] Physics Department, A.G & S.G Siddhartha Degree College of Arts and Science, Vuyyuru, 521165, India
[b] Physics Department, Andhra University, Visakhapatnam, 530003, India
[c] Physics Department, PBN College, Nidubrolu, 522124, India
[d] Physics Department, IIIT, RGUKT, Nuzvid, 521202, India
[e] Department of Medical Devices, National Institute of Pharmaceutical Education and Research (NIPER)-Ahmadabad, Palaji, Gandhinagar, 382355, India
[f] Physics Department, VFSTR (Deemed to be University), Vadlamudi, 530045, India

ARTICLE INFO

Keywords:
Ferrite nanoparticles
Superparamagnetic
Magnetic hyperthermia
Citric acid coating
Cell viability

ABSTRACT

The paper describes how to arrive at the required characteristics suitable for the study of magnetic hyperthermia in a nanoferrite. The composition selected for the study, $Ni_{0.60}Zn_{0.35}Fe_{2.05}O_4$ was synthesized by sol-gel process with an adequate control on its particle size using a chelating agent, polyethylene glycol (PEG). Nanoparticles with mean particle sizes in the range 3.6–8.2 nm were obtained by annealing the as-prepared powder at different temperatures. Identification of single phase spinel structure, particle size determination and magnetic properties of all the samples were made available with X-ray diffraction, Transmission electron microscopy, and Vibration sample magnetometer. The single domain nature of the nanoparticles was established from the particle size dependence of the coercivity. The superparamagnetic behaviour of two annealed samples having a mean particle sizes 3.6 nm and 4.4 nm was established from the temperature dependence of the field cooling and zero field cooling magnetization curves. The observed higher blocking temperature (below room temperature) for smaller particles was attributed to interactions between the particles in the powder samples. The effect of interparticle interactions on heating efficiency was examined by comparing the specific absorption rate (SAR) of nanoparticles dispersed in water at different concentrations. The higher zeta potential values of citric acid coated nanoparticles were pronouncing their long time stability in water with increased SAR and cell viability as compared to their uncoated counterparts. Interestingly, the results of water based citric acid coated nanoparticles assure that the material would be suitable as magnetic mediator for magnetic hyperthermia application.

1. Introduction

In recent years, due to the advances in the synthesis and characterization of the materials, the quest for novel magnetic nanoparticles useful for biomedical applications has attracted many researchers [1–3]. In the magnetic hyperthermia process, magnetic nanoparticles are administered into cancer affected tumour and excited with an alternating magnetic field to heat the tumour, such that the temperature of the tumor is maintained in the range 42 °C–46 °C at least for half an hour [4] to kill the cancer cells of many types without damaging the living cells. For this purpose, magnetic nanoparticles of least particle size, exhibiting superparamagnetic, or single domain ferri or ferromagnetic nature with negligible coercivity, sufficiently high specific saturation magnetization, biocompatibility, good dispersion stability in water medium and yielding a therapeutic temperature range for a longer time are desired.

Despite the fact that the heating efficiency of nanoparticles used for magnetic hyperthermia is dependent on saturation magnetization [5], the commonly used magnetic nanoparticles for magnetic hyperthermia application, magnetite and maghemite, although, possess superior biocompatibility [6], the disadvantage of their reduced saturation magnetization associated with the smaller sized particles opens research activity for better materials. On the other hand, the high saturation magnetization possessed by ferromagnetic metal nanoparticles like, iron,

* Corresponding author. Physics Department, A.G & S.G Siddhartha Degree College of Arts and Science, Vuyyuru, 521165, India.
** Corresponding author.
E-mail addresses: ramanavph69@gmail.com (P.V. Ramana), govindphysics@gmail.com (G. Kapusetti).

https://doi.org/10.1016/j.matchemphys.2021.124546
Received 14 July 2020; Received in revised form 12 March 2021; Accepted 22 March 2021
0254-0584/

cobalt, and nickel, made their usage impractical for biomedical applications due to their high toxicity and sensitivity to oxidation [7]. Even though, the use of nanoparticles of magnetic alloys MnZnFe, CoGdZn, and ZnGdFe is preferred over magnetic oxides for biological applications; the degree of toxicity is found substantial in the case of patients, exposed repeatedly to gadolinium-based compounds [8].

Earlier, ferrite nanoparticles MFe_2O_4 (M = Co, Ni, Zn, Mg, Cu, Mn) were studied for magnetic hyperthermia applications due to their structural stability and significant magnetic properties with limited outcome [9–14]. Nowadays, mixed ferrite nanoparticles with composition $M_{1-x}Zn_xFe_2O_4$ (M = Co, Ni, Mn) have been in limelight to find their use as heat mediators in magnetic fluid hyperthermia because of their preparation through eco-friendly routes, lower toxicity, size dependent magnetic properties, and attaining superior magnetic properties with an appropriate zinc concentration (x) [15–17]. Although, nickel-zinc ferrite nanoparticles have been studied extensively for various applications, the magnetic hyperthermia experiments conducted, so far are limited.

The heating efficiency of the magnetic nanoparticles in the presence of an alternating magnetic field has been characterized by the specific absorption rate (SAR), which is defined as the amount of energy converted into heat per unit mass per unit time. The SAR value is directly affected by external parameters such as frequency, amplitude of the applied magnetic field, the viscosity of the medium, and concentration of the nanoparticles, besides the intrinsic magnetic properties like saturation magnetization, magnetic anisotropy etc., which in turn depend on the preparation method of the nanoparticles. Ghayour et al. [16] studied $Ni_{1-x}Zn_xFe_2O_4$ (x = 0.25, 0.5 and 0.75) and reported that the samples having a higher saturation magnetization exhibit higher SAR in alternating magnetic field. Nanoparticles of higher SAR are essential in clinical hyperthermia to minimize the dosages of the material administered into a tumor in reaching the therapeutic temperatures.

Expecting higher saturation magnetization in larger sized particles is not a surprise, but development of least sized magnetic nanoparticles with high specific saturation magnetization requires meticulous concentration in the method of preparation. Xia Li et al. [18] processed superparamagnetic $Ni_{0.5}Zn_{0.5}Fe_2O_4$ nanopartices of size ranging from 6 nm to 19 nm with saturation magnetization less than 38 emu/g by hydrothermal method. Thakur et al. [19] made an attempt in preparing superparamagnetic $Ni_{0.58}Zn_{0.42}Fe_2O_4$ nanoparticles of sizes 8.4 nm, 14 nm and 17 nm by reverse micelle technique at different pH values and reported respective smaller values of saturation magnetization 25.63, 21.21 and 5.14 emu/g in 40 kOe applied magnetic field. By adopting sol-gel method with a proper chelating agent, several ferrite systems were processed and studied by the authors [17,20,21]. For the first time, the highest room temperature saturation magnetization, 80 emu/g was reported in $Ni_{0.65}Zn_{0.35}Fe_2O_4$ having particle size 42 nm [22]. A very high room temperature specific saturation magnetization, 91.9 emu/g for particle size 10.8 nm was reported in $Ni_{0.60}Zn_{0.35}Fe_{2.05}O_4$ [21].

Another important aspect of magnetic hyperthermia study is to maintain the therapeutic temperature range for a longer time and the findings of a few reports based on magnetic hyperthermia experiments were mentioned here. $Ni_{0.25}Zn_{0.75}Fe_2O_4$ nanoparticles [23] with high saturation magnetization and low coercivity were observed to yield therapeutic temperature range for a very short interval of time in an alternating magnetic field of amplitude 250 Oe, and 112 kHz frequency. In $Ni_{1-x}Zn_xFe_2O_4$ (x = 0.0 to 1.0) for $x \leq 0.5$, the fluid temperature was observed to grow to its boiling temperature in short interval of time, while the samples with $x \geq 0.8$ did not even reach the therapeutic temperature range [5]. In another study, the $Ni_{0.7}Zn_{0.3}Fe_2O_4$ superparamagnetic nanoparticles of size 11 nm prepared by the sol-gel method were observed to reach 43 °C within 7 min under an alternating magnetic field of frequency 7 MHz, and amplitude 400 Oe [24].

One more important feature in the study of magnetic hyperthermia is the tendency of agglomeration among nanoparticles due to their large surface energy as well as magnetic interactions between them which causes colloidal instability and hinders their practical application towards hyperthermia agents. The detachment can be accomplished by coating the surface of the nanoparticles with suitable organic/inorganic materials, or polymers. The surface coatings prevent agglomeration by generating an adequate repulsive force between the particles [25]. Further, the coating improves colloidal stability and provides accessible surface for conjugation of biomolecules and drugs. In recent years, efforts have been made by many research groups to prevent colloidal particles from aggregation by employing different polymer coatings on various kinds of magnetic nanoparticles [26–28]. Citric acid, a widely used coating material, provides high density coating over the surface of the nanoparticles due to its short chain, and enhances the dispersibility of nanoparticles in water [28].

Having understood the above facts and published a paper on cobalt-zinc nanoferrite, $Co_{0.37}Zn_{0.63}Fe_2O_4$ for self-regulating hyperthermia at temperature 46 °C [17], it has been thought of exploring the usefulness of nickel-zinc ferrite nanoparticles in a systematic way for the study of magnetic hyperthermia. In the present work, $Ni_{0.60}Zn_{0.35}Fe_{2.05}O_4$ nanoparticles have been synthesized by sol-gel method using PEG as chelating agent. Different particle sizes have been produced by annealing the as-prepared powder at different temperatures under extremely careful monitoring conditions. The samples with requisite properties to conduct hyperthermia experiment have been studied to understand the effect of dipolar interactions on heating efficiency by varying particle concentration (inter-particle distance) and frequency of applied alternating magnetic field. Further, the samples are coated with citric acid to reduce the interactions, to improve biocompatibility and colloidal stability in water. Finally, the usefulness of the coated nanoparticles for the study of magnetic hyperthermia was investigated by maintaining the therapeutic temperature range for a longer time.

2. Experimental details

2.1. Synthesis and characterization

The details of the sol-gel process, adopted in synthesizing $Ni_{0.60}Zn_{0.35}Fe_{2.05}O_4$ nanoparticles were described in earlier publications [17,21]. The as-prepared powder was made into 6 samples and annealed each at every 100 °C for 1 h in between 300 °C and 800 °C to understand the formation of domains and other size-dependent properties as a function of annealing. The samples were designated as NZ3, NZ4, NZ5, NZ6, NZ7 and NZ8 respectively throughout the paper.

The complete elimination of chelating agent, polyethylene glycol (PEG) from the samples was found by TG and DSC data. The crystal structure of the samples was established by irradiating them with Cu-K_α radiation (λ = 1.5406 Å) at the lowest scan rate of 0.02° per second, using a PANalytical X'Pert powder X-ray diffractometer. Transmission electron micrographs were recorded on a microscope (JOEL JEM 200CX model) with the electron operating voltage at 120 kV to estimate the particle sizes and their distribution. Fourier transform infrared (FTIR) spectrometer (PerkinElmer model 1650) was used to record the spectra of all the samples in the range 300–4000 cm^{-1} by kBr pellet method. Room temperature hysteresis loops were obtained using vibrating sample magnetometer (Lake Shore 7410S), operated at the maximum applied magnetic field of 15 kOe. Superparamagnetic nature was supported by the study of ZFC and FC curves, recorded using vibration sample magnetometer in the temperature range from 20 K to 300 K. Zeta potentials of uncoated and citric acid coated nanoparticles were measured using Malvern Zetasizernano zs90. The heating process of uncoated nanoparticles of varying concentrations 12 mg/mL, 16 mg/mL and 20 mg/mL under an AC magnetic field of amplitude 200 Oe was

carried out at two frequencies 519 kHz and 746 kHz using the magnetic induction heating instrument Magnetherm (make Nanotherics Limited, UK. Software-Magne Soft). In case of coated particles, magnetic induction heating was carried out for nanoparticle concentration12 mg/mL under the field of 200 Oe at both the frequencies 519 kHz and 746 kHz.

2.2. Cell viability assay

The MTT (4, 5-dimethylthiazol-2-yl-2, 5-diphenyl tetrazolium bromide) assay was performed to determine the cytotoxicity of uncoated and coated samples with mean particle sizes 3.6 nm and 4.4 nm with different concentrations (12, 16 and 20 mg/mL). The A549 (lung cancer cell line) cells with a density of 1×10^5 cm^{-2} were seeded on previously sterilized nanopowders in 24 well culture plates with 1 mL of MEM in triplicate and incubated for 24, 48 and 72 h at 37 °C. Following the incubation, 50 mL of 5 mg/mL MTT solution was added to the culture plates and incubated for another 4 h at 37 °C to produce formazan. Further, 100 mL of DMSO (Himedia, Mumbai, India) was added to MTT-containing medium to solubilize the formazan. The formazan solubilized solution was measured for optical density by using a multi-plate reader (Thermo Scientific – Varioskan Lux) at 560 nm with the help of the software package SkanIt RE 4.1. The percentage of cell viability has been estimated using the equation

$$\text{Cell viability (\%)} = \frac{\text{Optical density of sample}}{\text{Optical density of control sample}} \times 100 \quad (1)$$

3. Experimental findings and discussion

3.1. TG/DSC study

The TG/DSC curves of the as-prepared ferrite powder, shown in Fig. 1 depict the decomposition process of the chelating agent and its complete elimination from the ferrite.

The endothermic peaks around 213 °C, 393 °C, and 532 °C in DSC curve represent the onset of ferrite crystallization, breakdown of PEG [29] and decomposition of residual compounds respectively. The weight loss shown in TG curve up to 700 °C and the constancy of weight thereafter suggests the formation of pure and stable nanoferrite takes place above this temperature. Thus, the thermal behaviour of the material indicates that NZ3 to NZ7 samples contain both the ferrite material as well as chelating agent whereas, NZ8 comprises of only the ferrite material. The presence of chelating agent in the samples annealed below 800 °C has been confirmed from the observed extra bands in the FTIR spectra, given in section 3.4.

3.2. Spinel structure and impurity phases

Fig. 2 shows X-ray diffraction patterns of all the samples of $Ni_{0.60}Zn_{0.35}Fe_{2.05}O_4$ ferrite nanoparticles. The single phase cubic structure has been identified in the samples NZ3, and NZ4 by indexing the diffraction peaks using JCPDS cards (08–0234). Additional impurity lines, marked with an asterisk were identified in the samples NZ5, NZ6, NZ7 and NZ8 and attributed to traces of iron oxide (JCPDS card number 89–8104), formed because of the atomic diffusion mechanism during annealing [21]. Further, the annealing treatment was found to improve the crystallization of the samples, as evidenced by increasing the sharpness and intensity of the diffraction peaks.

3.3. TEM micrographs

The TEM micrographs of the samples and their respective particle size distribution (inset of micrographs) have been presented in Fig. 3. The particles of all the samples appear to be spherical with slight agglomeration. In estimating the particle size, Image J software has been used considering the linear dimensions of several particles of two image pictures at different regions of each sample. The particle size distribution is fitted with a log-normal function to evaluate the mean size of the particle. The average particle size of the sample has been observed to increase gradually from 3.6 nm to 8.2 nm, with increasing the annealing temperature and the standard deviation obtained from the fit, varies from 0.2 to 0.3. The particle size values are shown in Table 1. The broader particle size distribution has been observed with increasing the annealing temperature.

The rise in thermal energy, in general, favours the growth of crystallization by reducing the crystal defects and relieving the internal stresses. Moreover, the observed average particle size reiterates the controlling act of the chelating agent in the preparation of the samples. The influence of annealing temperature on the growth of the particle size runs parallel to the other systems discussed by many researchers [20,22].

The slight agglomeration caused by the high surface energy and magnetic interactions between the nanoparticles of uncoated samples may affect the magnetic heating efficiency in the study of magnetic hyperthermia. The problem may be solved by coating the surface of the nanoparticles using a suitable coating agent.

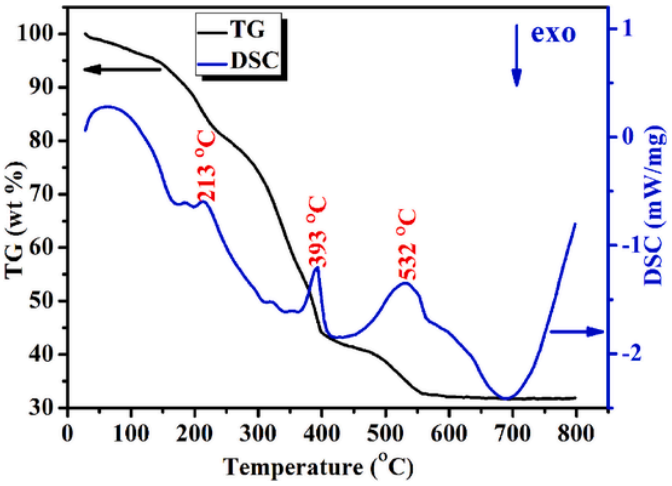

Fig. 1. TG/DSC curves of as-prepared powder.

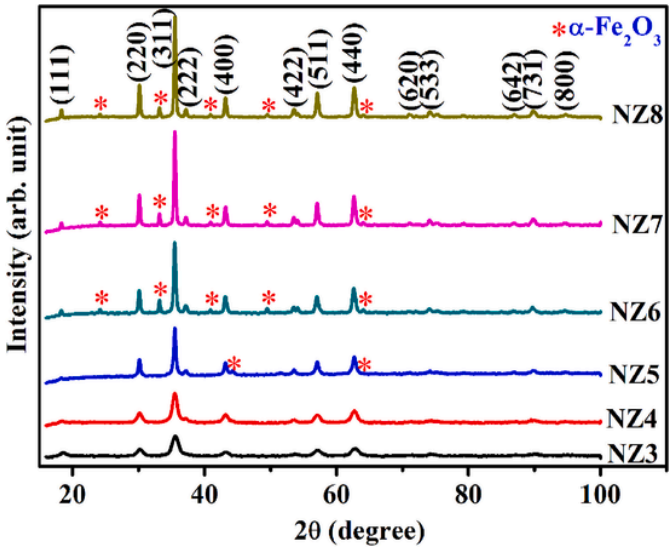

Fig. 2. X-ray diffractograms of nanoparticle samples, NZ3 to NZ8.

3.4. Complete elimination of the chelating agent

The FTIR spectra of all the samples, shown in Fig. 4 reveal two prominent metal-oxygen bands which correspond to the vibration modes of Fe^{3+} - O^{2-}bonds in the tetrahedral sites (observed range 568–590 cm^{-1}) and octahedral sites (observed range 404–411 cm^{-1}) [30]. The absorption bands that reveal the formation of the cubic spinel structure are in agreement with the XRD results of the samples.

The observed peaks at 1624 and 1363 cm^{-1} correspond to the vibrations of the carboxylate group (COO^{-}); validate the presence of PEG in the samples NZ3 to NZ7. Further, the gradual decrease of the peak intensity of the carboxylate group has been due to the depletion of the chelating agent from the nanoparticles. The disappearance of carboxylate group bands in the sample NZ8 is a clear indication of the complete removal of PEG from the material and the sample contains only the ferrite material. The broadband at about 3390 cm^{-1} is ascribed to stretching mode of the O–H group in the free and absorbed water [31].

3.5. Specific saturation magnetization

Room temperature magnetic hysteresis loops of all the samples are shown in Fig. 5 and the relevant magnetic parameters drawn from these loops are presented in Table 1. An initial noticeable increase from NZ3 to NZ4, unchanging fixed value in NZ4 to NZ7 and a steep rise to a very large value in NZ8 were noticed in relation to the specific saturation magnetization.

The net specific saturation magnetization of a magnetic nanoparticle, in general, is dependent on magnetic contributions from the surface spins and the core of the particle. The core of the nanoparticle is composed of magnetically ordered spins which align antiparallel due to super exchange interactions between the cations occupied both the tetrahedral and octahedral sites of the spinel structure. However, the surface atoms experience different environments due to several types of defects that exist on the surface, which include the existence of canted spins, changes in the atomic coordination, and lattice disorder. The uncompensated spin structure and the lack of symmetry at the surface of the particle develop surface anisotropy, which reduces the magnetic contribution of the surface as compared to that of the core.

As discussed in the previous section 3.1, the sample NZ3 annealed at 300 °C contains the ferrite material and larger amount of the chelating agent. The observed less specific saturation magnetization (30.8 emu/g) was attributed to the lesser amount of ferrite material present in the particle. The initial increase in specific saturation magnetization from NZ3 to NZ4 samples (30.8–36.3 emu/g) might be due to the increasing amount of ferrite material and reducing amount of the chelating agent caused by the rise in annealing temperature. An impurity phase of antiferromagnetic hematite (α-Fe_2O_3) was observed to grow in the samples NZ5 to NZ7 with the increase of annealing temperature. The presence of impurity phase, the leftover chelating agent and the surface anisotropy of the nanoparticles might be the responsible factors for keeping almost the same value of specific saturation magnetization in the samples NZ4 to NZ7. The complete elimination of a chelating agent, the presence of complete ferrite material in particles, the particle size growth and the consequent exchange interactions are pertinent causes for the observed steep rise in specific saturation magnetization in NZ8 sample.

Specifically, the insignificant remanent magnetization (σ_r) and coercivity (H_c) of NZ3 and NZ4 samples allow establishing the superparamagnetic behaviour of the samples, if any. In carrying out the hysteresis loop measurements, the applied magnetic field, 15 kOe was thought of insufficient to produce the saturation as the magnetization appeared to increase with the increase of the applied magnetic field. The incomplete saturation (inset of Fig. 5) has been asserted to be an indication of the presence of superparamagnetic single domain particles [32,33].

3.6. Single domain nature

The transition to the single domain state of multi domain structure due to annealing can be understood from the coercive field versus particle size curve as shown in Fig. 6. The size of the particle for which the maximum H_c occurs is known as critical size of the single domain particle and is around 5.1 nm which separates both the multi-domain and single-domain states. The nanoparticles having a particle size below 5.1 nm are single domain particles and above which are multi-domain particles. The observed variation of H_c is in consonance with those reported by many researchers [20,34,35].

Below the critical size, the increase in H_c with the particle size has been due to increasing magnetic anisotropy and the magneto-static energy of the particle is too low to form a domain wall with which the particle remains in the single-domain state. In the absence of domain wall, the spin rotation responsible for the magnetization reversal results in larger H_c of the nanoparticles. The observed decrease in H_c above the critical size has been attributed to the contributions that arise from the development of domain walls in the particles [20,36]. In multi-domain, the magnetization increases due to domain wall displacement under the action of the magnetic field.

In general, biocompatible superparamagnetic or low coercive single domain ferro/ferrimagnetic nanoparticles with sufficiently high saturation magnetization are desirable for the study magnetic hyperthermia. The samples NZ3 and NZ4 are considered to be superparamagnetic based on their insignificant values of remanent magnetization and H_c. The experiments conducted in establishing such nature are presented in the next section. The colloidal stability, biocompatibility and the heating efficiency of these nanoparticles were examined to explore their use as a potential material in magnetic hyperthermia.

3.7. Superparamagnetic nature

The magnetic moment of a superparamagnetic particle with all its spins aligned internally keeps flipping due to thermal energy. On cooling, the flip rate drops suddenly at some temperature where the magnetization of a superparamagnetic particle becomes frozen, and the corresponding temperature is called blocking temperature, a characteristic property of superparamagnetism. The blocking temperature has been measured from the temperature dependence of the zero-field cooling (ZFC) and field cooling (FC) magnetization curves for the nanoparticles of two samples NZ3 and NZ4. Fig. 7 shows the temperature dependence of ZFC and FC specific magnetizations (M_{ZFC} and M_{FC}) for both the samples at an applied magnetic field 500 Oe in the temperature range 20 K–300 K.

From the ZFC curves, it is evident that the specific magnetization rises gradually up to a maximum and then decreases with increasing temperature. The temperature at which specific magnetization reaches a maximum, viz, T_{max}, is known as blocking temperature of the system. The observed blocking temperatures are 100 K for NZ3 and 201 K for NZ4 having a mean particle sizes 3.6 nm and 4.4 nm respectively. Larger the particle size higher the magnetic anisotropy energy and hence higher thermal energy is required for superparamagnetic transition. These values are higher than those reported by Xia Li et al. [18] for $Ni_{0.5}Zn_{0.5}Fe_2O_4$ nanoparticles of size 6 nm in a magnetic field of 500 Oe.

The bifurcation of ZFC and FC magnetization curves occurs at a certain temperature known as irreversibility temperature, T_{irr}, determined at a point on the curves where the common acceptable condition, $(M_{FC}-M_{ZFC})/M_{FC} < 1\%$ is fulfilled [37]. The irreversibility temperatures, thus obtained for NZ3 and NZ4 samples are 131 K and 261 K respectively. The irreversibility temperature is an essential characteristic of the superparamagnetic system [19], above which the ZFC and FC curves superimpose in both the samples. Generally, in a system containing monosize, and non-interacting superparamagnetic nanoparticles, the T_{irr} co-

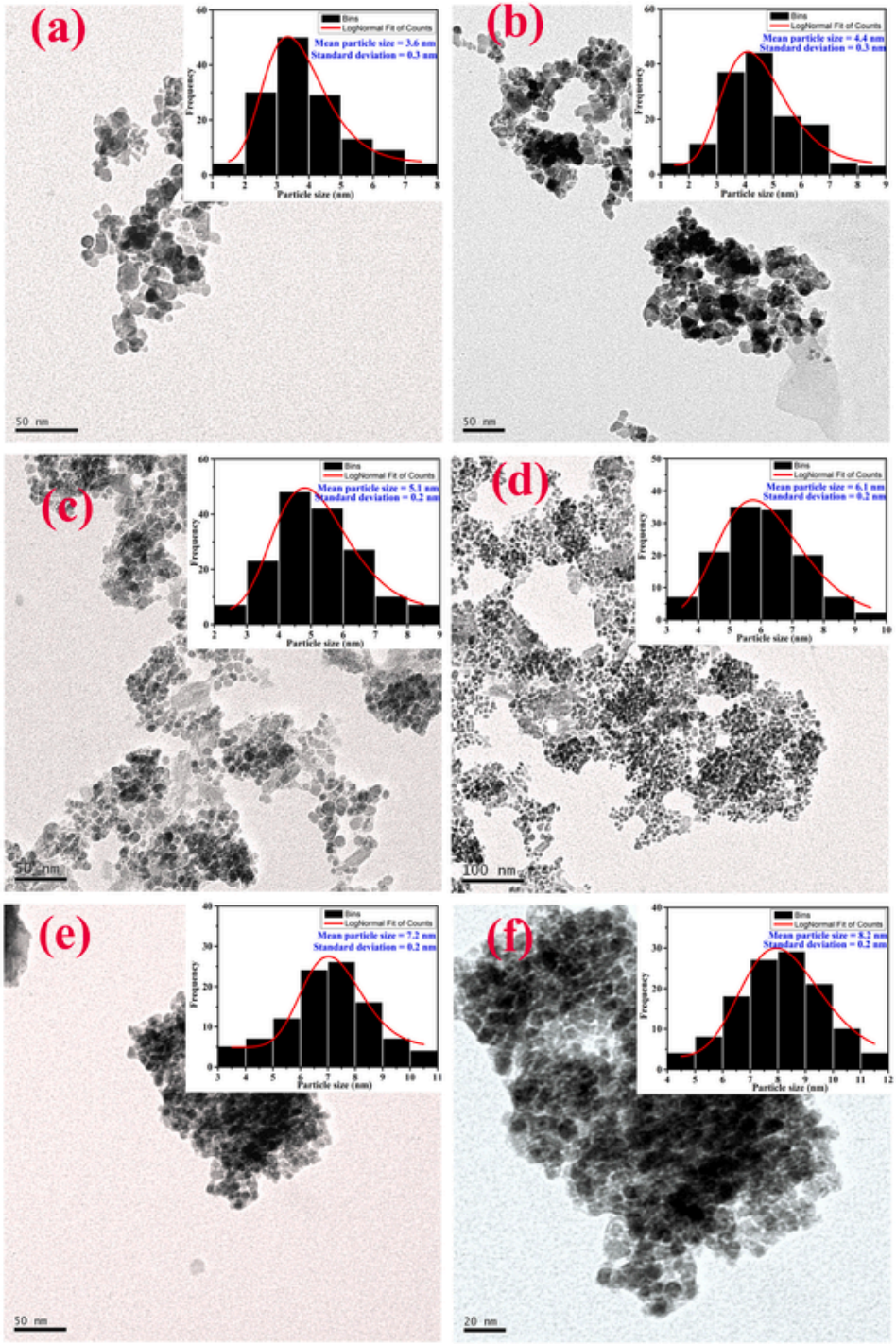

Fig. 3. TEM images and particle size distribution of the samples, NZ3 (a) –NZ8 (f).

Table 1
Particle size, specific saturation magnetization (σ_S), remanent magnetization (σ_r) and coercive field (H_c) for all the samples.

Sample	Particle size (nm)	σ_S (emu/g)	σ_r (emu/g)	H_c (Oe)
NZ3	3.6	30.8	0.16	7
NZ4	4.4	36.3	0.77	27
NZ5	5.1	35.8	4.39	113
NZ6	6.1	35.4	4.48	112
NZ7	7.2	35.1	4.44	106
NZ8	8.2	84.2	7.39	90

incides with T_{max} and the ZFC magnetization curve shows a sharp peak. However, the broad maximum of the ZFC curve and the separation between T_{irr} and T_{max} indicate the particle distribution and interaction between the nanoparticles [38]. Further, the closeness of T_{irr} and T_{max} in NZ3 sample is associated with the narrow size distribution of the particles as observed by TEM leading to the existence of less magnetic interactions between the particles as compared to those of NZ4 sample. The magnetic interactions between the particles contribute an additional energy to the effective anisotropy, and require higher thermal energy for superparamagnetic transition. Therefore, the blocking temperature shifts towards the higher temperature values in both NZ3 and NZ4 samples. Several researchers have reported higher blocking temperatures in

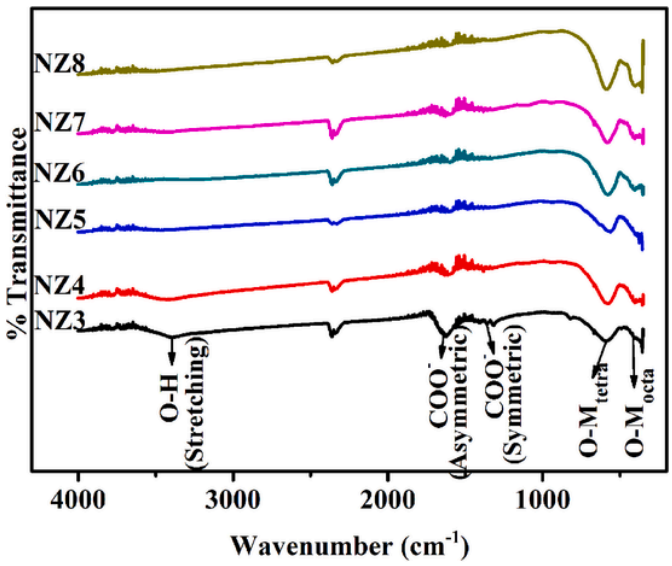

Fig. 4. FTIR spectra of the samples, NZ3 to NZ8.

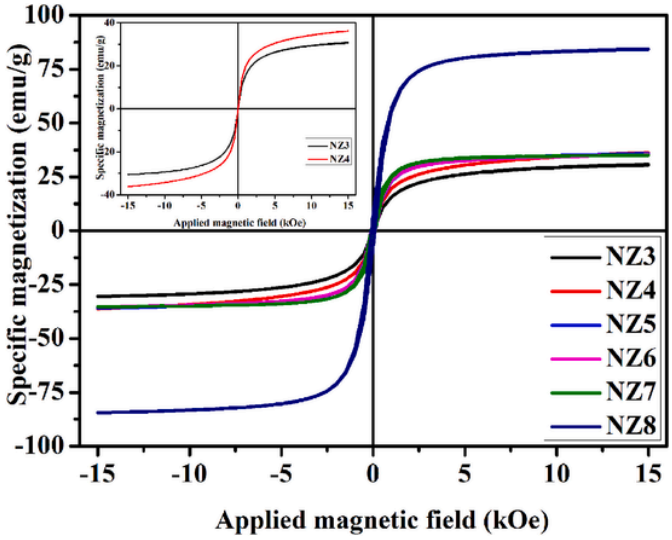

Fig. 5. M–H loops of all samples, NZ3 to NZ8, at room temperature.

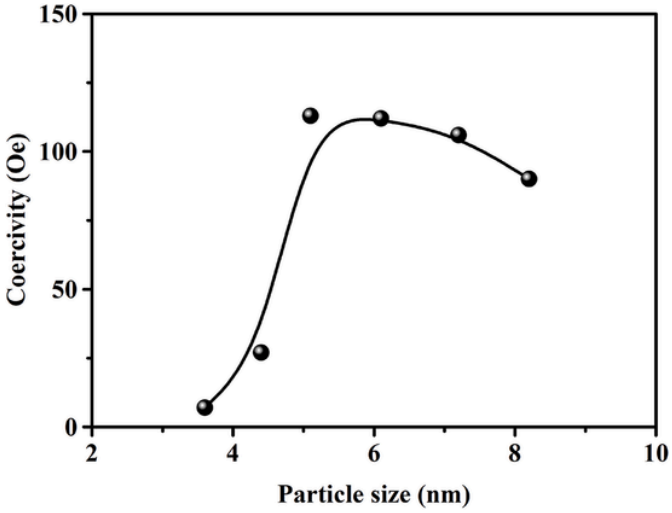

Fig. 6. Particle size dependence of coercivity.

the systems having interacting superparamagnetic nanoparticles [39–41].

3.8. Colloidal stability

The magnetic nanoparticles with good dispersion and colloidal stability over a long time period in the water near the neutral pH are essential for biomedical applications. The colloidal stability of the nanoparticle in water dispersion has been studied through zeta potential measurement and the values for NZ3 and NZ4 nanoparticles at pH 7 have been found to be – 18.9 mV and – 9.07 mV respectively. The negative potential of the nanoparticle is leading to the existence of negatively charged carboxylate groups over the surface of the particle as observed by the respective absorption bands in the FTIR spectrum. The zeta potential of NZ3 nanoparticles is more negative than NZ4 nanoparticles, leading to their less aggregation, thus providing relatively higher colloidal stability in water.

3.9. Magnetic hyperthermia experiment

The heating efficiency of superparamagnetic nanoparticles, NZ3 and NZ4 has been tested using induction heating experiment, choosing an alternating magnetic field of amplitude 200 Oe at two frequencies 519 kHz and 746 kHz for varied concentrations 12 mg/mL, 16 mg/mL and 20 mg/mL of the sample in a water medium. The self-heating temperature characteristic curves are given in Fig. 8 and Fig. 9.

With an initial sharp rise, the temperature of the specimen shows a gradual increase with time under the specified conditions. However, the rise of temperature to a higher value in a short interval of time is seen with increasing concentration and frequency.

Generally, the temperature rise with time in the induction heating process is ascribed to the heat produced by the particles through magnetic losses under alternating magnetic field. The high resistivity of ferrite nanoparticles keeps the losses due to eddy currents at minimum. The rapid changes in the direction of the magnetic moment of the particle due to the field, generate heat via Néel relaxation, while, the hindrance of particle rotation within the liquid viscous force generates heat due to Brownian relaxation.

The heating ability of the magnetic material, evaluated by the specific absorption rate (SAR) of the dispersed nanoparticles in water is given by the following expression [25],

$$SAR = C\left(\frac{dT}{dt}\right)\left(\frac{m_S}{m_m}\right) \quad (2)$$

where, C is the specific heat capacity of water (4.186 J/g °C), m_S and m_m represent the masses of the suspension and the nanoparticles in the suspension respectively. The maximum of the derivative $(\frac{dT}{dt})$that occurs within a few seconds has been considered to be the best approximation of the adiabatic character of the measurement [42].

The maximum SAR was observed for NZ3 nanoparticles at both the frequencies, 519 KHz and 746 kHz whereas, for NZ4 nanoparticles only at 519 kHz for the concentrations 16 mg/mL. In the case of the NZ4 sample, SAR has been observed to decrease with increasing concentration from 123.8 W/g to 48.4 W/g at 746 kHz (inset of Fig. 9b). The decrease in SAR with the increasing concentration has previously been reported by several researchers [9,15,43]. The SAR value is known to depend on several parameters, viz. frequency and amplitude of the alternating magnetic field, the amount and dispersion of the sample in the suspension besides its properties [18]. The large SAR associated with NZ4 for the concentration 12 mg/mL at 746 kHz might be due to the combined contributions from Brownian and/or Néel loss. The higher the concentration, the smaller the interparticle distance results in improving the magnetic interactions between the particles and consequent decrease in Néel and Brownian relaxation losses on heat leading to a low SAR. The SAR values obtained above 60 W/g for a given set of

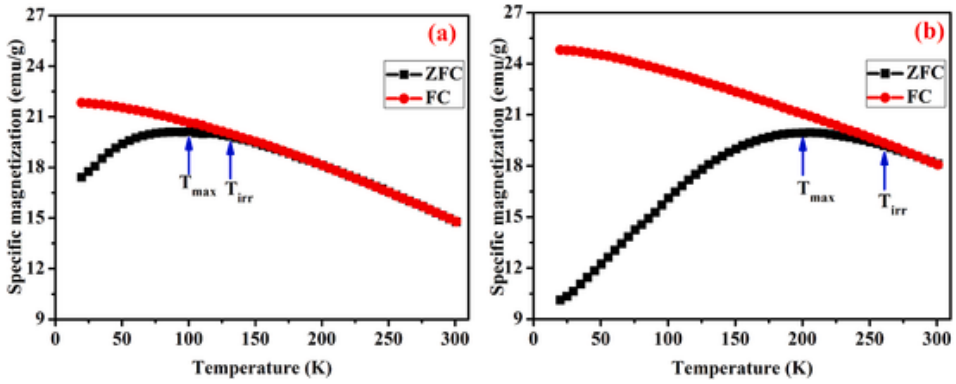

Fig. 7. Variation of ZFC-FC magnetization (a) NZ3 and (b) NZ4 nanoparticles in an applied magnetic field of 500 Oe.

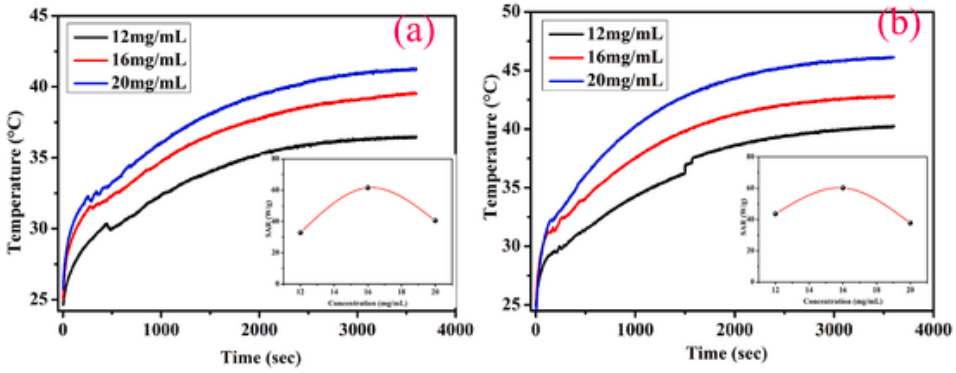

Fig. 8. Temperature versus time curves of (a) NZ3 and (b) NZ4 under the magnetic field 200 Oe at frequency 519 kHz.

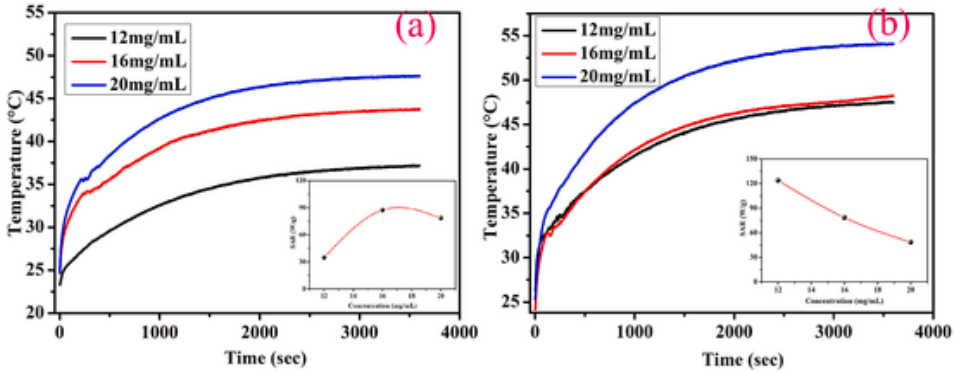

Fig. 9. Temperature versus time curves of (a) NZ3 and (b) NZ4 under the magnetic field 200 Oe at frequency 746 kHz.

concentration and frequency are acceptable to those of the materials used for magnetic hyperthermia [5].

3.10. Cytotoxic effect of nanoparticles on A549 cells

The MTT assay was performed to understand the biocompatibility of NZ3, and NZ4 nanoparticles. The study was conducted with A549 cell line with a time interval of 1, 3, and 7 days. The observed cell viability was above 90% in all the samples on day one. The same trend was observed on day three and seven (Fig. 10). The Ni–Zn ferrites were reported for the potential cytotoxicity even at μg/mL concentrations [44]. Interestingly, the particles of higher concentration have shown well bio-compatibility. The possible reason may be the chelation of nanoparticles with highly biocompatible PEG which reduces the cytotoxicity in NZ3 and NZ4 samples.

The present study corroborates that experimentation with larger amount of magnetic material is not imperative to attain higher value of

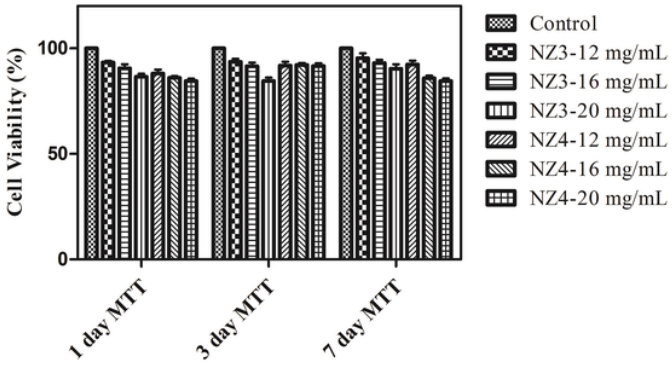

Fig. 10. Cell viability of NZ3 and NZ4 nanoparticles with different concentrations.

SAR. However, the SAR should be as high as possible to minimize the concentration of the nanoparticles used for magnetic hyperthermia under the acceptable alternating magnetic field and frequency [34].

Further, several studies reveal that the surface coating plays an important role in colloidal stability and bio-compatibility which ultimately change the performance of the magnetic hyperthermia material [45,46]. The surface coating in general, prevents the formation of aggregates by maintaining proper distance through electrostatic repulsion between the particles [25].

3.11. Effect of coating

With a view of eliminating agglomeration of the nanoparticles, if any, the samples NZ3 and NZ4 have been coated with citric acid to produce superior magnetic fluid hyperthermia agents.

The surface of the nanoparticles was modified with carboxylic groups by coating with citric acid. Briefly, 4 mL of citric acid solution was prepared in de-ionized water with a concentration of 0.5 mg/mL. Simultaneously, 50 mL of nickel-zinc ferrite nanoparticle dispersive solution in water was prepared with a concentration of 1 mg/mL. The slurry of magnetic nanoparticles was heated to 90 °C and added with previously prepared citric acid solution by continuous stirring for 1 h. Finally, the coated nanoparticles were retrieved by magnetic decantation, washed with water and dried in the vacuum oven for 24 h [47,48]. The final products, so obtained are designated as CANZ3 and CANZ4 in the following sections.

The citric acid layer formed on the surface of the nanoparticles of the samples may be identified from the additional bands present in the FTIR spectra. Fig. 11 shows FTIR spectra of pure citric acid, CANZ3, and CANZ4 nanoparticles. No significant variation is seen in the FTIR spectra of CANZ3 and CANZ4 nanoparticles.

The pure citric acid absorption bands are clearly resolved and a few bands appear in the coated samples with low intensity. The absorption band 1724 cm^{-1} has been assigned to the C = O vibration from COOH group of citric acid. The complete disappearance of the peak 1724 cm^{-1} and appearance of a new band 1585 cm^{-1} in the samples correspond to the vibrations of carboxylate (COO^-) group; validate the binding of polymer on the surface of the magnetic nanoparticles through a COOH group of citric acid [49]. The observed decrease in the intensity of the peaks has been thought of due to the formation of carboxylate group complexes with the iron atoms on the surface of the magnetic nanoparticles. The absorption bands 1380 cm^{-1} and 1228 cm^{-1} have been assigned to the stretching of COO^- and C–O groups of citric acid respectively [50]. Further, relatively an intense band observed around 591 cm^{-1} is due to the vibration mode of Fe^{3+} - O^{2-} bond in the tetrahedral site of magnetic nanoparticles [50].

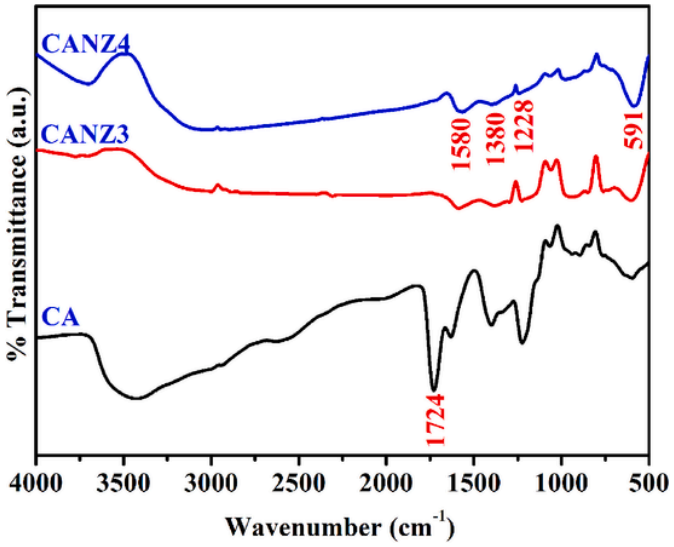

Fig. 11. FTIR spectra of pure citric acid, CANZ3, and CANZ4 nanoparticles.

The presence of citric acid on the nanoparticles was further confirmed by the zeta potential values. The zeta potential values for CANZ3 and CANZ4 nanoparticles at pH 7 are – 27.1 mV and – 35.7 mV respectively. The negative value suggests the presence of negatively charged carboxylate groups on the surface of the nanoparticles. The observed higher values as compared to those of NZ3 and NZ4 nanoparticles are attributed to the creation of an additional negative surface charge due to citric acid coating. The negative charges on the surface of the nanoparticles oppose agglomeration of the particles due to repulsive forces between the particles which enables the long time stability in water.

Fig. 12 shows the significant increase in cell viability in CANZ3 and CANZ4 nanoparticles when compared to NZ3 and NZ4 nanoparticles at all concentrations due to the presence of carboxylate groups on the surface of the nanoparticles. Li. et al. [48] also reported an improved biocompatibility in citric acid coated iron oxide nanoparticles even at higher concentrations of the material.

Further, both the uncoated and coated nanoparticles have shown no toxicity even at higher concentration 20 mg/mL.

3.12. SAR values of uncoated and coated nanoparticles

The heating efficiency of CANZ3 and CANZ4 nanoparticles was examined under an alternating magnetic field of amplitude 200 Oe at 519 kHz and 746 kHz for particle concentration 12 mg/mL in a water medium. For a clear understanding of the effect of citric acid coating on SAR, the heating efficiency of NZ3 and NZ4 nanoparticles for concentration 12 mg/mL has been compared with that of CANZ3 and CANZ4 nanoparticles. The self-heating temperature characteristic curves of NZ3, NZ4, CANZ3 and CANZ4 nanoparticles at both the frequencies are given in Fig. 13 and Fig. 14.

The basic process of magnetic hyperthermia is the interaction between the magnetic moment of the nanoparticle and applied time-varying magnetic fields. Heat is generated through three important mechanisms, namely Néel relaxation, Brownian relaxation and loss of hysteresis [51]. How much energy is released depends on the frequency and amplitude of the applied magnetic field, as well as the intrinsic magnetic properties of the nanoparticles. The heating ability of the magnetic nanoparticles is dependent on its size, shape, composition, coated layer and specific absorption rate.

Heat loss in the case of small nanoparticles can be due to Néel relaxation and the Brownian contribution can be overlooked. To reach high heating levels, Néel relaxation should not be allowed to dominate. The VSM results of the NZ3 and NZ4 samples (section 3.5) show hysteresis loops with negligible remanent magnetization and coercivity (Table 1) probably due to agglomeration and larger particle size. The contribu-

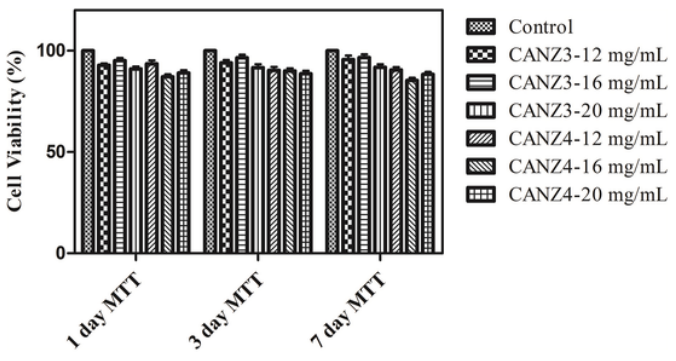

Fig. 12. Cell viability of CANZ3 and CANZ4 nanoparticles with different concentrations.

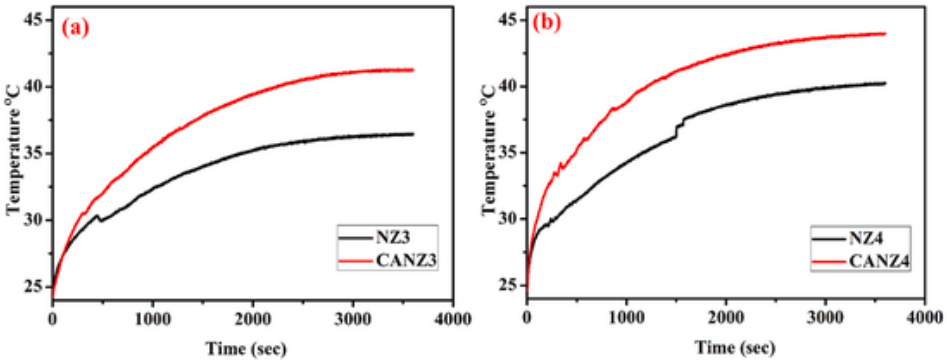

Fig. 13. Heating abilities of (a) NZ3 and CANZ3 and (b) NZ4 and CANZ4 nanoparticles for concentration 12 mg/mL at 519 kHz.

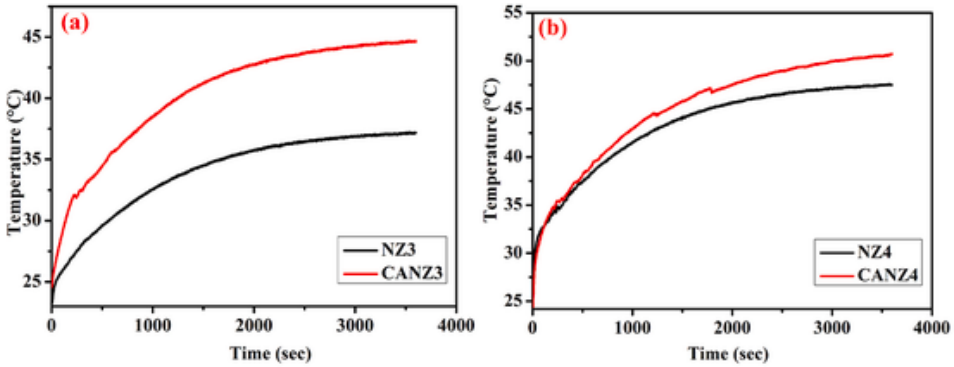

Fig. 14. Heating abilities of (a) NZ3 and CANZ3 and (b) NZ4 and CANZ4 nanoparticles for concentration 12 mg/mL at 746 kHz.

tion of hysteresis loss can be anticipated for these samples in addition to Néel relaxation [51,52]. Achieving the therapeutic temperature range in NZ4 nanoparticles is attributed to the additional loss of hysteresis over NZ3 nanoparticles.

Uncoated NZ3 nanoparticles did not produce the therapeutic temperature at the two frequencies investigated in the experiment, while uncoated NZ4 nanoparticles provided the required therapeutic temperature range at 746 kHz. However, the CANZ3 and CANZ4 coated samples achieved the therapeutic temperature even at 519 kHz. The temperature reaches a maximum after a certain time, because the heat generated is balanced by the loss of heat of the nanoparticle system. From Figs. 13 and 14 for nanoparticle concentration 12 mg/mL, the temperature change (17.1 °C–26.3 °C) shown by the coated particles is more than that provided by uncoated particles (11.9 °C–21.2 °C) for an hour exposure of magnetic field at both the frequencies. Furthermore, the SAR values of both coated and uncoated nanoparticles at two frequencies, presented in Table 2, clearly establish the significance of the coating.

For the same concentration of nanoparticles, the same frequency and the same amplitude of the magnetic field, the initial temperature increase is higher in nanoparticles coated compared to uncoated particles dispersed in the water medium. As a result, SAR values show higher heating efficiency for coated nanoparticles compared to uncoated particles. The citric acid surface coating which enables higher SAR values, prevents the agglomeration of nanoparticles and provides good dispersion stability compared to the uncoated nanoparticles.

From the results of the FTIR and zeta potentials (section 3.11), it is believed that the complete binding of the citric acid coating provides more negative charge due to the presence of the COO^-group on the surface of the magnetic nanoparticles. An adequate thickness of the citric acid coating keeps the approaching nanoparticles far by allowing sufficient electrostatic repulsion between the nanoparticles and establishing the balance among the nanoparticles. Consequently, coated nanoparticles have been distributed homogeneously in water medium and exhibit a good colloidal stability for a long time without significant change in particle size. The efficiency of heat generation is thus increased for the well dispersed coated nanoparticles through Néel and Brownian relaxations and several researchers also reported higher SAR values for efficiently dispersed nanoparticles [41,53–56].

The SAR values of the coated nanoparticles of the present study are shown in Table 3 along with others' work to elucidate the heating efficiency of citric acid coating. From the comparison of SAR and the product of magnetic field amplitude (H) and frequency (f) values, it is evident that citric acid coated Ni–Zn ferrite nanoparticles of concentration 12 mg/mL are assured to be promising candidates for their use in magnetic fluid hyperthermia as heating agents in providing the required therapeutic temperature range for adequate time.

As per the recent reports, the maximum field-frequency product that living tissues tolerate varies from $1.8 \times 10^9 Am^{-1}s^{-1}$to $18.7 \times 10^9 Am^{-1}s^{-1}$ [60–62] and the product of the present work is within the range of the reported values. At the end, the study indicates that the citric acid coating has greatly improved biocompatibility and stability of nanoparticles in water medium for longer time with distinct SAR values.

Table 2
SAR values of uncoated and coated nanoparticles for concentration 12 mg/mL.

Frequency (kHz)	SAR (W/g)		SAR (W/g)	
	NZ3	CANZ3	NZ4	CANZ4
519	32.8	41.7	43.6	64
746	34.8	42.6	123.8	131.5

Table 3
Comparison of SAR and Hf values under specified conditions.

Nanoparticles	f (kHz)	H (kA/m)	Particle concentration (mg/mL)	SAR (W/g)	**Hf ($Am^{-1}s^{-1}$)**	Reference
Citric acid coated $Ni_{0.6}Zn_{0.35}Fe_{2.05}O_4$	519	15.91	12	64	8.25×10^9	Present study
Citric acid coated $Ni_{0.6}Zn_{0.35}Fe_{2.05}O_4$	746	15.91	12	131.5	11.86×10^9	Present study
Citric acid coated magnetite	293	60	30	42	17.58×10^9	[57]
Triethylene glycol coated $Ni_{0.6}Zn_{0.4}Fe_2O_4$	216	4.4	10	50	0.95×10^9	[58]
Dextron coated $MgFe_2O_4$	265	26.7	10	55.6	7.08×10^9	[13]
Terephthalic acid (TA) - 2-aminoterephthalic acid (ATA) coated superparamagnetic iron oxide nanoparticles	751.5	10.9	8	126	8.2×10^9	[59]

H values are represented in kA/m. Here 1 kA/m = 12.566 Oe.

4. Conclusions

The method adopted in processing the nanoparticles was proved to be an efficient one in reducing the size of the particles to the extent of exhibiting superparamagnetic single domain nature. The occurrence of heating ability close to 46 °C for nearly 35 min was demonstrated for uncoated samples of different concentrations 12 mg/mL, and 16 mg/mL in an alternating magnetic field 200 Oe at a frequency 746 kHz by conducting magnetic induction heating experiments. In case of coated nanoparticles, the required therapeutic temperature range was observed at a frequency 519 kHz for concentration 12 mg/mL in an alternating magnetic field 200 Oe. The cytotoxicity study on lung cancer cell line evinced greater cell viability of the coated samples for all different concentrations of the nanoparticles. Hence, the present study favours the suitability of citric acid coated nickel-zinc ferrite superparamagnetic nanoparticles for magnetic hyperthermia application.

Declaration of competing interest

The authors declared that they have no known competing financial interests or personal relationships that could have appeared to influence the work reported in this paper.

Acknowledgments

The authors acknowledge the help rendered by the concerned staff of IIT Madras, NIT Warangal and CCMB for providing the TG/DSC, VSM, XRD and TEM facilities.

References

[1] M. Coïsson, G. Barrera, C. Appino, F. Celegato, L. Martino, A.P. Safronov, G.V. Kurlyandskaya, paola Tiberto, J. Magn. Magn Mater. 473 (2019) 403–409.
[2] E. Mazarío, J. Sánchez-Marcos, N. Menéndez, A. Mayoral, S. Rivera-Fernández, J.M. de la Fuente, P. Herrasti, Magdalena Cañete, J. Phys. Chem. C 119 (2015) 6828–6834.
[3] Z. Shaterabadi, G. Nabiyouni, M. Soleymani, Prog. Biophys. Mol. Biol. 133 (2018) 9–19.
[4] D. Kim, D.E. Nikles, D.T. Johnson, C.S. Brazel, J. Magn. Magn Mater. 320 (2008) 2390–2396.
[5] A.I. Tovstolytkin, M.M. Kulyk, V.M. Kalitab, S.M. Ryabchenko, V.O. Zamorskyi, O.P. Fedorchuk, S.O. Solopan, A.G. Belous, J. Magn. Magn Mater. 473 (2019) 422–427.
[6] M. Suto, Y. Hirota, H. Mamiya, A. Fujita, R. Kasuya, K. Tohji, B. Jeyadevan, J. Magn. Magn Mater. 321 (2009) 1493–1496.
[7] NhiemTrana, Thomas J. Webster J. Mater. Chem. 20 (2010) 8760–8767.
[8] M. Rogosnitzky, S. Branch, Biometals 29 (2016) 365–376.
[9] P.T. Phong, N.X. Phuc, P.H. Namd, N.V. Chien, D.D. Dung, P.H. Linh, Phys. B Condens. Matter 531 (2018) 30–34.
[10] A. Doaga, A.M. Cojocariu, W. Amin, F. Heib, P. Bender, R. Hempelmann, O. F. Caltun, Mater. Chem. Phys. 143 (2013) 305–310.
[11] S. Bae, S. Won Lee, Y. Takemura, Appl. Phys. Lett. 89 (2006) 252503.
[12] S. Manjura Hoque, Md, S. Hossain, S. Choudhury, S. Akhter, F. Hyder, Mater. Lett. 162 (2016) 60–63.
[13] V.M. Khot, A.B. Salunkhe, N.D. Thorat, R.S. Ningthoujam, S.H. Pawar, Dalton Trans. 42 (2013) 1249–1258.
[14] L. Khanna, G. Gupta, S.K. Tripathi, Mater. Sci. Eng. C 97, 2019, pp. 552–566.
[15] P.H. Nam, N.X. Phuc, P.H. Linh, L.T. Lu, D.H. Manh, P.T. Phong, In-Ja Lee, Physica B: Condensed Matter 550 (2018) 428–435.
[16] H. Ghayour, M. Abdellahi, N. Ozada, S. Jabbrzare, J. Amirsalar Khandan, Phys. Chem. Solids 111 (2017) 464–472.
[17] P. Appa Rao, K. Srinivasa Rao, T.R.K. Pydi Raju, G. Kapusetti, M. Choppadandi, M. Chaitanya Varma, K.H. Rao, J. Alloys Compd. 794 (2019) 60–67.
[18] X. Li, J. GuisuWang, Magn. Magn. Mater 321 (2009) 1276–1279.
[19] S. Thakur, S.C. Katyal, M. Singh, J. Magn. Magn Mater. 321 (2009) 1–7.
[20] K. Srinivasa Rao, S.V. RangaNayakulu, M. Chaitanya Varma, G.S.V.R.K. Choudary, K.H. Rao, J. Magn. Magn Mater. 451 (2018) 602–608.
[21] P.V. Ramana, K. Srinivasa Rao, K.H. Rao, J. Magn. Magn Mater. 465 (2018) 747–755.
[22] A. Mahesh Kumar, M. Chaitanya Varma, CharuLataDube, K.H. Rao, S.C. Kashyap, J. Magn. Magn Mater. 320 (2008) 1995–2000.
[23] H. Choi, Hyung Joon Kim, J. Magn. Magn Mater. 484 (2019) 14–20.
[24] Seung Wha Lee, Chul Sung Kim J. Magn. Magn Mater. 304 (2006) e418–e420.
[25] A.B. Salunkhe, V.M. Khot, J.M. Ruso, S.I. Patil, J. Magn. Magn Mater. 419 (2016) 533–542.
[26] T. Zargar, A. Kermanpur, S. Labbaf, A. Baharlou Houreh, M.H. Nasr Esfahani, Mater. Chem. Phys. 212 (2018) 432–439.
[27] R.J. Wydra, A.M. Kruse, Y. Bae, K.W. Anderson, mater. Sci. Eng. C 33 J. Zach Hilt 2013, pp. 4660–4666.
[28] S. Munjal, N. Khare, B. Sivakumar, D.N. Sakthikumar, J. Magn. Magn Mater. 477 (2019) 388–395.
[29] Z. Huanque, H. Fei, Z. Xuelin, S. Qiangqiang, P. Huifen, J. Qang Xin, Magn. Magn. Mater 439 (2017) 245–250.
[30] M.M. Mallapur, P.A. Shaikh, R.C. Kambale, H.V. Jamadar, P.U. Mahamuni, B.K. Chougule, J. Alloys Compd. 479 (2009) 797–802.
[31] C. Sujatha, K. Venugopal Reddy, K. Sowri Babu, A. Rama Chandra Reddy, K. H. rao, Ceram. Int. 38 (2012) 5813–5820.
[32] I. Sharifi, H. Shokrollahi, J. Magn. Magn Mater. 334 (2013) 36–40.
[33] M. Chithra, C.N. Anumol, BaidyanathSahu, S.C. Sahoo, J. Magn. Magn Mater. 424 (2017) 174–184.
[34] V. Kumar, A. Rana, M.S. Yadav, R.P. Pant, J. Magn. Magn Mater. 320 (2008) 1729–1734.
[35] W.S. Chiu, S. Radiman, R. Abd-Shukor, M.H. Abdullah, P.S. Khiew, J. Alloys Compd. 459 (2008) 291–297.
[36] B.G. Toksha, S.E. Shirsath, S.M. Patange, K.M. Jadhav, Solid State Commun. 147 (2008) 479–483.
[37] V. Kusigerskia, E. Illesa, J. Blanusa, S. Gyergyek, M. Boskovic, M. Perovic, J. Vojislav Spasojevic, Magn. Magn. Mater 475 (2019) 470–478.
[38] Y. Köseoğlu, Ceram. Int. 39 (2013) 4221–4230.
[39] S. YPHe, Q. Wang, C. R Li, Z. YMMiao, Y. Wu, B. S Zou, J. Phys. D Appl. Phys. 38 (2005) 1342–1350.
[40] X. Li Liu, E. Shi Guang Choo, A.S. Ahmed, L.Y. Zhao, Y. Yang, R.V. Ramanujan, J. Min Xue, D. Di Fan, H. Ming Fan, J. Jun Ding, Mater. Chem. B 2 (2014) 120–128.
[41] A. Tomitaka, T. Koshi, S. Hatsugai, T. Yamada, J. Yasushi Takemura, Magn. Magn. Mater 323 (2011) 1398–1403.
[42] E. Lima Jr., T.E. Torres, L.M. Rossi, H.R. Rechenberg, T.S. Berquo, A. Ibarra, C. Marquina, M.R. Ibarra, G.F. Goya, J nanopart Res 15, 2013, p. 1654.
[43] P.T. Phong, P.H. Nam, D.H. Manh, J. In-Ja Lee, Magn. Magn. Mater 433 (2017) 76–83.
[44] M.S. Al-Qubaisi, A. Rasedee, M.husein Flaifel, S.H.J. Ahmad, M. Zobir Hussein, E. EM Eid, Z. Zainal, M. Saeed, S. Fakurazi, N. Mohd Isa, M.E. El Zowalaty, Munallowefah, Samer hussein-Al-Ali Int. J. Nanomed. 8 (2013) 2497–2508.
[45] V.M. Khot, A.B. Salunkhe, N.D. Thorat, R.S. Ningthoujam, S.H. Pawar, Dalton Trans. 42 (2013) 1249–1258.
[46] R.M. Patil, N.D. Thorat, P.B. Shete, S.V. Otari, B.M. Tiwale, S.H. Pawar, Mater. Sci. Eng. C 59, 2016, pp. 702–709.
[47] C.J. Pandian, R. Palanivel, U. Balasundaram, J. Photoch. Photobio. B 174, 2017, pp. 58–69.

[48] L. Li, K.Y. Mak, C.W. Leung, K.Y. Chan, W.K. Chan, W. Zhong, P.W.T. Pong, Microelectron. Eng. 110 (2013) 329–334.
[49] M. Racuciu, D.E. Creang„ A. Airinei, Eur. Phys. J. E 21, 2006, pp. 117–121.
[50] S. Nigam, K.C. Barick, D. Bahadur, J. Magn. Magn Mater. 323 (2011) 237–243.
[51] M.E. Sadat, R. Patel, J. Sookoor, S.L. Bud'ko, R.C. Ewing, J. Zhang, H. Xu, Y. Wang, G.M. Pauletti, D.B. Mast, D. Shi, Mater. Sci. Eng. C 42 (2014) 52–63.
[52] K.D. Bakoglidis, K. Simeonidis, D. Sakellari, G. Stefanou, M. Angelakeris, IEEE Trans. Magn. 48 (2012) 1320–1323.
[53] S.V. Jadhav, D.S. Nikam, S.S. Mali, C.K. Hong, S.H. Pawar, New J. Chem. 38 (2014) 3678–3687.
[54] P. Das, M. Colombo, Davide Prosperi, Colloids and Surfaces B: Biointerfaces 174 (2019) 42–55.
[55] S.V. Jadhav, D.S. Nikam, V.M. Khot, S.S. Mali, C.K. Hong, S.H. Pawar, Mater. Char. 102 (2015) 209–220.
[56] S.V. Jadav, D.S. Nikam, V.M. Khot, N.D. Thorat, M.R. Phadatare, R.S. Ningthoujam, A.B. Salunkhe, S.H. Pawar, New J. Chem. 37 (2013) 3121–3130.
[57] R.A. Frimpong, J. Dou, M. Pechan, J. Zach Hilt, J. Magn. Magn Mater. 322 (2010) 326–331.
[58] A. Ahmad, H. Bae, I. Rhee, J. Sungwook Hong, Magn. Magn. Mater 447 (2018) 42–47.
[59] G. Kandasamy, A. Sudame, P. Bhati, A. Chakrabarty, J. Dipak Maity, Mol. Liq 256 (2018) 224–237.
[60] Z. Hedayatnasab, F. Abnisa, W.M. Ashri, Wan Daud Mater. DES 123 (2017) 174–196.
[61] Y. Oh, N. Lee, H. Wook Kang, J. Oh, Nanotechnology 27 (115101) (2016) 21.
[62] E. Garaio, J.M. Collantes, J.A. Garcia, F. Plazaola, S. Mornet, F. Couillaud, O. Sandre, J. Magn. Magn Mater. 368 (2014) 432–437.